Tuning the magnetic properties of a VSe_2 monolayer via the magnetic proximity effect mediated by Zeeman-type spin-orbit interaction

Mahsa Abdollahi and Meysam Bagheri Tagani*
Department of Physics, University of Guilan, P. O. Box 41335-1914, Rasht, Iran

(Received 19 January 2023; accepted 10 July 2023; published 26 July 2023)

Intrinsic room-temperature ferromagnetic ordering and inversion asymmetry of V-based transition metal dichalcogenide (TMD) monolayers with trigonal prismatic coordinates are highly desirable to develop spintronic devices. Motivated by facilitating the performance improvement of V-based TMDs in data-storage applications, we investigated the influence of the interface magnetic proximity effect, mediated by Zeeman-type spin-orbit interaction (SOI), on the magnetic exchange interaction and magnetic anisotropy of the 2H-VSe_2 monolayer. It has already been observed that strain and interlayer coupling does not have a significant effect on the magnetic anisotropy of V-based TMDs. Here we demonstrate using density functional theory (DFT) that the proximity effect of the archetypal metallic material $NbSe_2$ at the van der Waals interface induces strong out-of-plane magnetic anisotropy in 2H-VSe_2. The transition of magnetization from in plane to out of plane in 2H-VSe_2 holds great promise toward the realization of faster and smaller magnetic bits in lower power-consuming memory devices such as random access memories. The valley polarization of the VSe_2 system is significantly reversed by applying Zeeman-type SOI of $NbSe_2$ substrate. Also, by combining the two-band $\boldsymbol{k}\cdot\boldsymbol{p}$ model with high-throughput DFT calculations, the change of $\boldsymbol{k}\cdot\boldsymbol{p}$ parameters of 2H-VSe_2 is examined due to Zeeman-type SOI induced by $NbSe_2$.

DOI: 10.1103/PhysRevB.108.024427

I. INTRODUCTION

A sizable magnetic anisotropy lays the cornerstone of stability of the long-range magnetic ordering in 2D materials by opening an excitation gap to resist the thermal agitation, which precludes the validity of the Mermin-Wagner theorem [1]. Since the appearance of magnetic anisotropy with a variety of sources such as magnetocrystalline anisotropy, shape anisotropy, and stress anisotropy in 2D magnetic atomic crystals, different magnetic models based on the Heisenberg model were used to justify the observed magnetization. Ultrathin $Cr_2Ge_2Te_6$ flakes with small magnetic anisotropy are 2D magnetic atomic crystals [2,3] which can be described by the so-called anisotropic Heisenberg model. Aligned spin moments have a small energy difference in the mentioned 2D systems, so they can be oriented in all directions. Moreover, the XY model is used to interpret the magnets of 2D $CrCl_3$ with easy plane anisotropy [4], which is a lattice model of classical spin vortices and waves related to the Berezenskii-Kosterlitz-Thouless transition [5]. The simplest model, the so-called Ising model [6], is used for describing highly anisotropic magnets with long-range frustrated ferromagnetic (FM) as well as antiferromagnetic (AFM) couplings. The Ising model was used to describe the experimentally observed magnetization in the monolayer CrI_3 [7].

The primary source of anisotropy, single-ion magnetocrystalline anisotropy, is derived from spin-orbit interaction (SOI). Manipulation of trajectories of electron spin by inducing strong SOI is a tempting and attractive concept in quantum phenomena such as topological insulators [8], spin-Hall effect [9], and ballistic conduction of spins [10]. Not only can the SOI weaken the paramagnetism effect but it can also enhance in-plane critical field, B_c, beyond the Pauli limit, B_p, [11,12] in ultrathin superconducting films [13–15]. Specifically, the antisymmetric form of spin-orbit coupling (SOC) due to the lack of inversion symmetry in crystals [16], plays a significant role in inducing the Rashba or Zeeman-type spin splitting. In a 2D system, Rashba-type SOI originating from out-of-plane inversion asymmetry aligns the spin of electrons within the x-y plane [17,18], and the critical field of the system, B_c, is lower than the Pauli limit [19,20]. On the other hand, Zeeman-type SOI or Ising-type SOI is allowed in a 2D system with broken in-plane inversion symmetry, causing an out-of-plane spin polarization of energy valleys [21–23]. Zeeman-type SOI in transition metal dichalcogenides (TMDs) such as $NbSe_2$ and MoS_2 monolayers with a trigonal prismatic structure (namely, H phase) leading to spin-polarized Fermi surface [19,24,25] and in-plane critical field can far exceed the Pauli limit [19,20,26].

Recently, the investigation of 2D van der Waals (vdW) heterostructures has been expanded to achieve the desired physical properties. For example, the perpendicular magnetic anisotropy of the NiI_2 monolayer is effectively enhanced by reducing the interlayer distance of graphene/NiI_2 heterostructures [27]. In WSe_2/CrI_3 heterostructures, degenerate energy levels of valleys are split into slightly lower and slightly higher energy levels due to the magnetic proximity effect, and a large magnetic field is obtained [28]. By reversing the direction of the ferroelectric polarization of In_2Se_3 in vdW

*m_bagheri@guilan.ac.ir

heterostructures, a FM/AFM phase transition is observed in FeI_2 [29]. In Ref. [30], a magnetic proximity effect in a gate-tunable $MoSe_2/CrBr_3$ heterostructure has been observed using resonance optical reflection spectroscopy, where the high quality of the interface leads to the giant zero-field valley splitting in $MoSe_2$, equivalent to an external magnetic field of 12 T. On the other hand, given the importance of SOI in the development of future spintronics devices, there has recently been an intense focus on dynamic and spatial modulation of SOI [31–33]. Especially, the proximity effect caused by the interfacial interaction of vdW TMD heterostructures is useful for inducing SOI [15,34,35] to the neighboring layer, which is a result of charge redistribution between the adjacent materials. The proximity effect of the nonmagnetic semiconductor monolayer $PtSe_2$ with large SOC has led to increases of magnetic anisotropy as well as Curie temperature, T_C, far beyond room temperature in $Cr_2Ge_2Te_6$ [36]. But, apart from the recent investigation presented in Ref. [37], there have been no experimental and theoretical studies reported on the effect of the Zeeman-type SOI on the magnetic properties of materials.

Investigation of the effect of Zeeman-type SOI on the magnetic exchange interaction as well as magnetic anisotropy of the VSe_2 monolayer is the main motivation for the present paper. Recently, the physical properties of the highly attractive VSe_2 monolayer have been extensively investigated, which is very different from properties of bulk phase, including strong FM order at room temperature [38,39] and CDW modulated structures [40,41]. Due to the fact that the 2H semiconductor phase of VSe_2 is thermodynamically more stable than the 1T metal phase in 2D and also the inversion and time-reversal symmetries are broken in the 2H phase, we chose the 2H phase in our study. Recently, monolayer 2H-VSe_2 nanoflakes were mechanically exfoliated from their single crystals [38]. On the other hand, the coupling of intrinsic FM and valley degrees of freedom in 2H-VSe_2 ferrovalley is important for us [42]. Recent studies have shown that the 2H-VSe_2 monolayer has in-plane magnetization [43]. Despite many studies on the challenging monolayer 2H-VSe_2, some questions still need to be answered. For example, how does Zeeman-type SOI affect the in-plane magnetic anisotropy of the 2H-VSe_2 monolayer? It has already been shown that data storage in perpendicular magnetic recording has higher density compared to longitudinal recording [44]. Later, research on materials with perpendicular magnetization began to increase the information processing speed of optical magnetic recorders and advanced spintronic devices such as resistive magnetoresistive random-access memory and magnetoresistive sensors [45,46].

In this paper, the electronic and magnetic properties of the $VSe_2/NbSe_2$ heterostructure are examined by first-principles density functional theory (DFT) calculations. Our calculations reveal that 2H-VSe_2 was switched from the XY ferromagnet to the Ising ferromagnet with strong anisotropy. So, application of VSe_2 is improved in nanoscale spintronic devices by attaching $NbSe_2$ as a substrate. Also, by combining the two-band $\boldsymbol{k}\cdot\boldsymbol{p}$ model with high-throughput DFT calculations, the change of the $\boldsymbol{k}\cdot\boldsymbol{p}$ parameters of the VSe_2 monolayer due to the Zeeman-SOI-mediated magnetic proximity effect has been investigated.

II. COMPUTATIONAL METHODS

The first-principles calculations using the projector-augmented wave [47] method have been carried out within the Perdew, Burke, and Ernzerhof [48] approximations of the exchange-correlation functional as implemented in the VIENNA AB INITIO SIMULATION PACKAGE (VASP) [49]. The first Brillouin zone is sampled with Γ centered Monkhorst-Pack grid [50] of 15×15×1 and 20×20×1 for the structure optimization and electronic structure calculations, respectively. The kinetic energy cutoff of plane wave basis is set as 500 eV, and a vacuum thickness of 20 Å along the z direction is utilized to avoid interaction between adjacent layers. The energy and force convergence criteria on each atom were less than 10^{-6} eV and 10^{-2} eV/Å for the fully relaxed initiating structures, respectively. The DFT-D3 method within the Grimme scheme was included in all calculations to consider the vdW forces [51]. Also, GGA+U calculations based on Dudarev's approach [52] are tested in VASP, with the effective on-site Coulomb interaction parameter $U = 1$, 2, and 3 eV for d orbitals of V atoms. To accurately estimate the magnetic anisotropy energy (MAE), SOC is included in a noncollinear mode [53] within self-consistent calculations after the structural relaxations. MAE, the energy difference between two directions of the magnetization, indicates in-plane and out-of-plane easy axes of a material.

III. ELECTRONICS AND MAGNETICS PROPERTIES OF VSe_2 MONOLAYER

A. Electronic structure

Figure 1(a) shows the structure of the 2H-VSe_2 monolayer. A lattice constant of 3.336 Å was obtained, which is in good agreement with theoretical and experimental results in Refs. [43,54–56]. V atoms are enclosed by six chalcogenide atoms in a trigonal prism with a point group symmetry of D_{3h} and the nearest V-Se distance is about 2.50 Å. The crystal field induced by the trigonal prism splits the d orbitals of the vanadium atom into three suborbitals including $a_1' = d_{z^2}$, $e' = d_{x^2-y^2}, d_{xy}$, and $e'' = d_{xz}, d_{yz}$. The a_1' state has the lowest energy level, and e' and e'' states are located above the Fermi energy [57,58]. So, one electron of V^{4+} ion completely fills the majority spin of $a_1' = d_{z^2}$ state, whereas the minority spin of all states and four majority spin of e' and e'' states are empty [59]. As a result, unit cell magnetization is equal to 1 μ_B, which is in accordance with the first Hund's rules. Characteristics of V-Se bonding are revealed by the top view of the electron localization function (ELF) contour map on the plane crossing V and Se atomic planes, as shown in Fig. 1(a). The highest ELF value is found near the V and Se atomic cores, indicating an ionic bonding nature of the V-Se interactions. Also, according to the side view of the electron density difference (EDD) map presented in Fig. 1(a), Se surface gains electron density and becomes negatively charged (the accumulation electron density represented by blue color), V atomic plane loses electron density and becomes positively charged (the depletion electron density represented by red color) [60].

Regardless of the SOI, VSe_2 is a bipolar magnetic semiconductor as shown in Fig. 1(b). The valence band maximum (VBM) and conduction band minimum (CBM) are located in

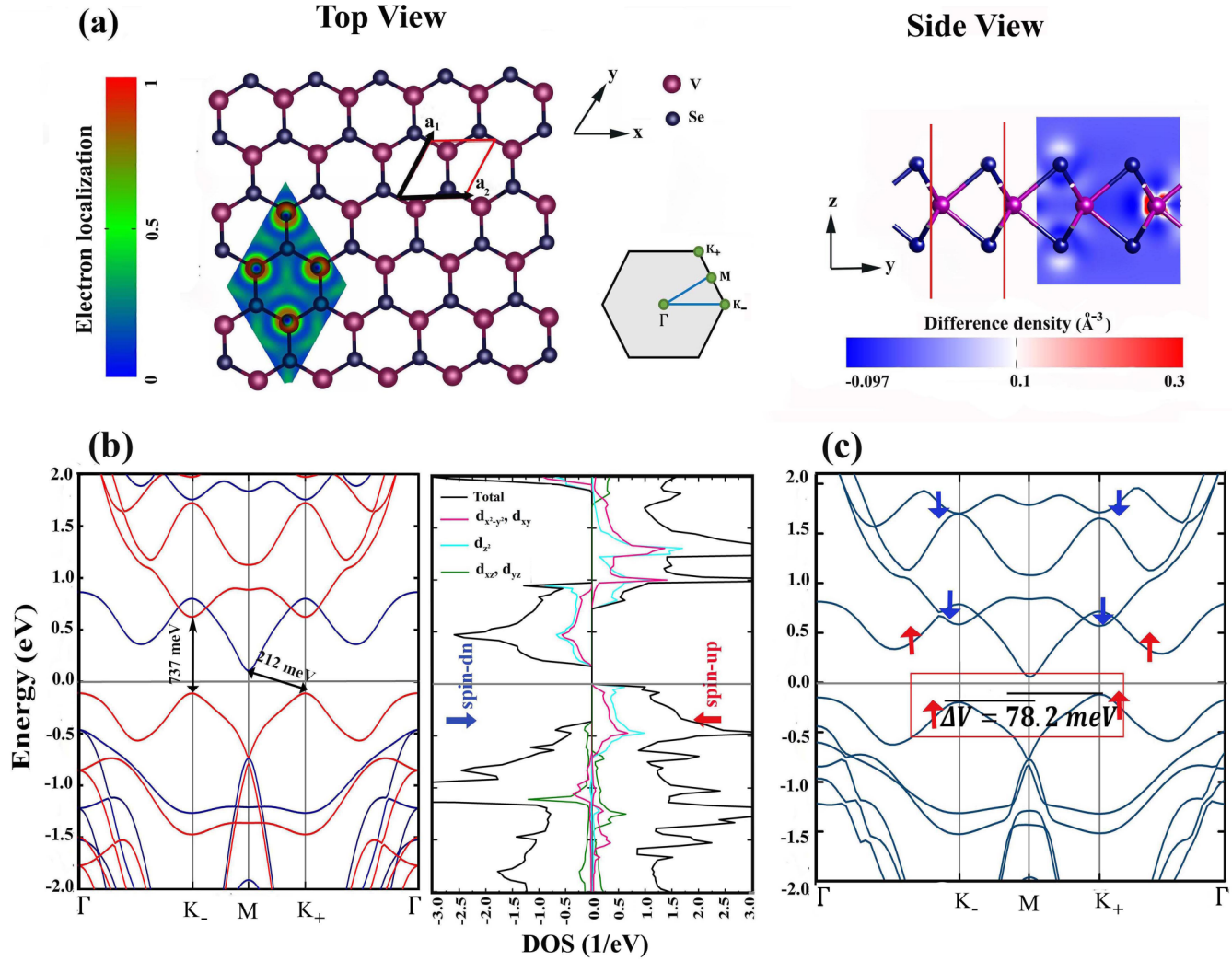

FIG. 1. (a) Crystal structure of 2H-VSe_2 monolayer with ELF and EDD contours in the plane and vertical to plane of 2H-VSe_2, respectively. Unit cell is also depicted in (a). (b) Spin-polarized band structure of 2H-VSe_2 monolayer for majority spin (up) and minority spin (down) without considering SOC effect and spin-resolved density of states (DOS) projected to different d orbitals of V atom. (c) The band structure by considering both the ferromagnetism and SOC effect.

the valleys $K_{+(-)}$ for the majority spin. Unlike MoS_2, spin-valley locking is not observed in the 2H-VSe_2 monolayer due to the breaking of time-reversal symmetry, coming from inherent magnetization. The band gap of the spin majority is 737 meV, and H-VSe_2 has an indirect band gap of 219 meV. The results obtained from the band structure calculations are in agreement with previous reports [43,61–63].

Analyzing the density of states shows that the edge of the valence and conduction bands is composed of d orbitals of the V atoms [Fig. 1(b)]. The d_{z^2} orbital plays a dominant role in the VBM while the d_{xy} and $d_{x^2-y^2}$ orbitals also participate in the edge of the conduction band. This orbital pattern at the edge of the valence and conduction bands is characteristic of all H-phase TMDs [62,64,65]. The difference in the orbital contribution in monolayer VSe_2 compared to nonmagnetic TMDs is due to exchange interactions and Hund's rules.

The combination of SOI, time-reversal symmetry breaking, and inversion-symmetry breaking leads to the emergence of valley polarization, as shown in Fig. 1(c). Due to the breaking of the time-reversal symmetry, the edge of the valence band for the majority spins is no longer equal in the two valleys and a 78.2 meV gap appears. The polarity of the valley in the conduction band is weaker and its value is 18 meV. The difference in the magnitude of valley polarization is directly related to the participation of different d orbitals. Due to the dominant states from the V atom in the band structure of 2H-VSe_2 (see Supplemental Material Fig. S1 [66]), orbital magnetic moment m_L along the z direction near the $K_\pm$ valleys is approximately equal to 0 and $\pm 2\ \mu_B$, at the edge of the conduction and valence bands, respectively. The spin magnetic moments of the valence-band edge parallel to the upward direction produces an effective magnetic field B_{eff} acting on the orbital magnetic moment ($m_L B_{\text{eff}}$). So, a significant up (down) energy shift ($2\ \mu_B\ B_{\text{eff}}$) occurs in the K_+ (K_-) valley of the valence band, while the energy shift does not occur in the valley's edge of the conduction band ($m_L B_{\text{eff}} = 0$). The band gap size is 690 meV in K_+ valley and 787 meV in K_- valley. This difference leads to the emergence of magnetic circular dichroism in the structure, which has recently been confirmed in experiments [67–69].

TABLE I. The values of the exchange interaction between the nearest J_1 and next-nearest neighbors J_2. D (T_C) represents the magnetic anisotropy (Curie temperature) of 2H-VSe_2 Monolayer.

Structure	J_1 (meV)	J_2 (meV)	D (meV)	T_C (K)
2H-VSe_2	89.7	−15.97	−0.586	427.81

B. Magnetic structure

Superexchange of 2H-VSe_2 monolayer with near-90° Se-V-Se bonds at the next-nearest neighbor (NNN) is always FM. Moreover, owing to the small overlap between a_1' subshells, the FM indirect exchange overcomes the AFM direct interaction between two neighboring V^{4+} ions, which is associated with the Pauli exclusion principle. Also, to calculate the computationally magnetic ground state and to understand the spin interactions, we use a spin Heisenberg model for a 2D magnetic honeycomb lattice as follows [70,71]:

$$H = -\sum_{i<j} J_{ij}\mathbf{S}_i \cdot \mathbf{S}_j - D\sum_i \left(S_i^z\right)^2, \tag{1}$$

where $\mathbf{S}_{i(j)}$ is the spin operator for the i^{th} (j^{th}) magnetic atom, J_{ij} is the symmetric Heisenberg exchange coupling between spins on sites i and j. D represents the magnetic anisotropy of the structure originating from spin-orbit interaction and $D > 0$ represents the easy axis perpendicular to the plane and $D < 0$ indicates the existence of the easy plane.

A rectangular grid with dimensions of (a, $\sqrt{3}$a) consisting of four vanadium atoms andeight selenium atoms is used to calculate symmetric exchange interactions for nearest neighbors (NNs), J_1, and NNNs, J_2, and magnetic anisotropy D. We consider three different spin arrangements including FM and AFM arrangements in which the vanadium atoms in a line have the same spin orientation (AFM_1), and AFM arrangements in which the vanadium atoms in a line alternate spin orientation (AFM_2). The different spin arrangements are shown in Fig. S2. The difference between the AFM_1 and AFM_2 configurations is in the spin interaction of the NNN. In the AFM_1 configuration, there are four AFM interactions between the NNN, while in the AFM_2 configuration, there are four FM interactions between the NNN.

Using Eq. (1) and the different spin arrangements considered, we can write the energy of the different spin configurations as follows:

$$\begin{aligned}
E^z_{(\text{FM})} &= E_0 - 12J_1S^2 - 12J_2S^2 - 4DS^2,\\
E^z_{(\text{AFM}_1)} &= E_0 + 4J_1S^2 + 4J_2S^2 - 4DS^2,\\
E^z_{(\text{AFM}_2)} &= E_0 + 4J_1S^2 - 4J_2S^2 - 4DS^2,\\
E^x_{(\text{FM})} &= E_0 - 12J_1S^2 - 12J_2S^2,
\end{aligned} \tag{2}$$

where E_0 denotes part of energy independent from spin interaction, E^x_{FM} is the energy of the supercell when the spin of V atoms are along the x direction, and $S = 1/2$. We have considered SOI and used noncollinear calculations to compute total energy of different spin arrangements.

The values of J_1, J_2, and D are listed in Table I, which shows that the ground state of the VSe_2 monolayer is FM in agreement with the reported results in Refs. [72–74]. As expected, J_1 is much larger than J_2, however, J_2 cannot be ignored. Another interesting point is the AFM interaction between the NNN. The amount of ion magnetic anisotropy was also negative, indicating that the VSe_2 monolayer has an easy plane anisotropy and follows the XY model. The values obtained for J_1, J_2, T_C, and D are consistent with previous reports [38,43,62,75], which confirms the accuracy of our calculations.

MAE is caused by SOI. To understand the in-plane magnetization of the VSe_2 monolayer, we examine the second-order contribution of SOI to empty and full states. The contributions to MAE can be divided into two parts: the participation of full and empty bands with the same spin and the participation of bands with opposite spins. The contribution of two parts is given as [76,77]

$$\Delta E_{\pm,\pm} = \left(\frac{\zeta}{2}\right)^2 \frac{|\langle o^{\pm}|L_z|u^{\pm}\rangle - \langle o^{\pm}|L_x|u^{\pm}\rangle|^2}{\epsilon_u - \epsilon_o}, \tag{3a}$$

$$\Delta E_{\pm,\mp} = \left(\frac{\zeta}{2}\right)^2 \frac{|\langle o^{\pm}|L_x|u^{\mp}\rangle - \langle o^{\pm}|L_z|u^{\mp}\rangle|^2}{\epsilon_u - \epsilon_o}, \tag{3b}$$

where $o^+(u^+)$ and $o^-(u^-)$ denote occupied (unoccupied) states for spin up and spin down, respectively. ζ is the spin-orbit strength of the V atom and $\epsilon_u - \epsilon_o$ is the energy difference between occupied and unoccupied states. It is clear from Fig. S1 that only the d orbitals of the V atom play a dominant role at the band edges. VBM consists of a hybrid of d_{z^2}, d_{xy}, and $d_{x^2-y^2}$ with spin up, while CBM has the same orbitals with spin down. Hence, the predominant sentence in MAE is $-\frac{\zeta^2\hbar^2}{\epsilon_{\text{CBM}}-\epsilon_{\text{VBM}}}$, which justifies in-plane magnetism of VSe_2 obtained from DFT calculations.

Linear dependence of T_C according to the exchange coupling parameters can derived from the mean-field approximation and the Heisenberg model with long-range interaction in Eq. (1) as [78–80]

$$T_C = \frac{2{\mu_S}^2}{3 * k_B}\sum_{i=1}^{2}\frac{n_i}{2}J_i, \tag{4}$$

where n_1 and n_2 represent the NN and NNN magnetic coordination numbers, respectively, where both coefficients in the hexagonal lattice of 2H-VSe_2 are equal to 6 [80,81]. μ_S and k_B are the total spin and the Boltzmann constant, respectively. As shown in Table I, the calculated T_C for 2H-VSe_2 is around 427.81 K, which is in good agreement with the experimental and DFT computational results stated in Refs. [38,75,82,83].

Despite the high Curie temperature, the existence of an easy plane anisotropy limits the application of VSe_2 monolayer in spintronics. It is very important that magnetic materials have an easy axis perpendicular to the plane, so their magnetic properties can be controlled with the help of external fields [84–87].

IV. ZEEMAN-TYPE SOI IN 2H-$NbSe_2$ MONOLAYER

Figure 2(a) shows the structure of 2H-$NbSe_2$ monolayer in which Nb atoms with a triangular lattice are sandwiched by two layers of Se atoms with the same lattice. We obtained the lattice constant of 3.47 Å for the 2H-$NbSe_2$ monolayer, in agreement with previous experimental and computational

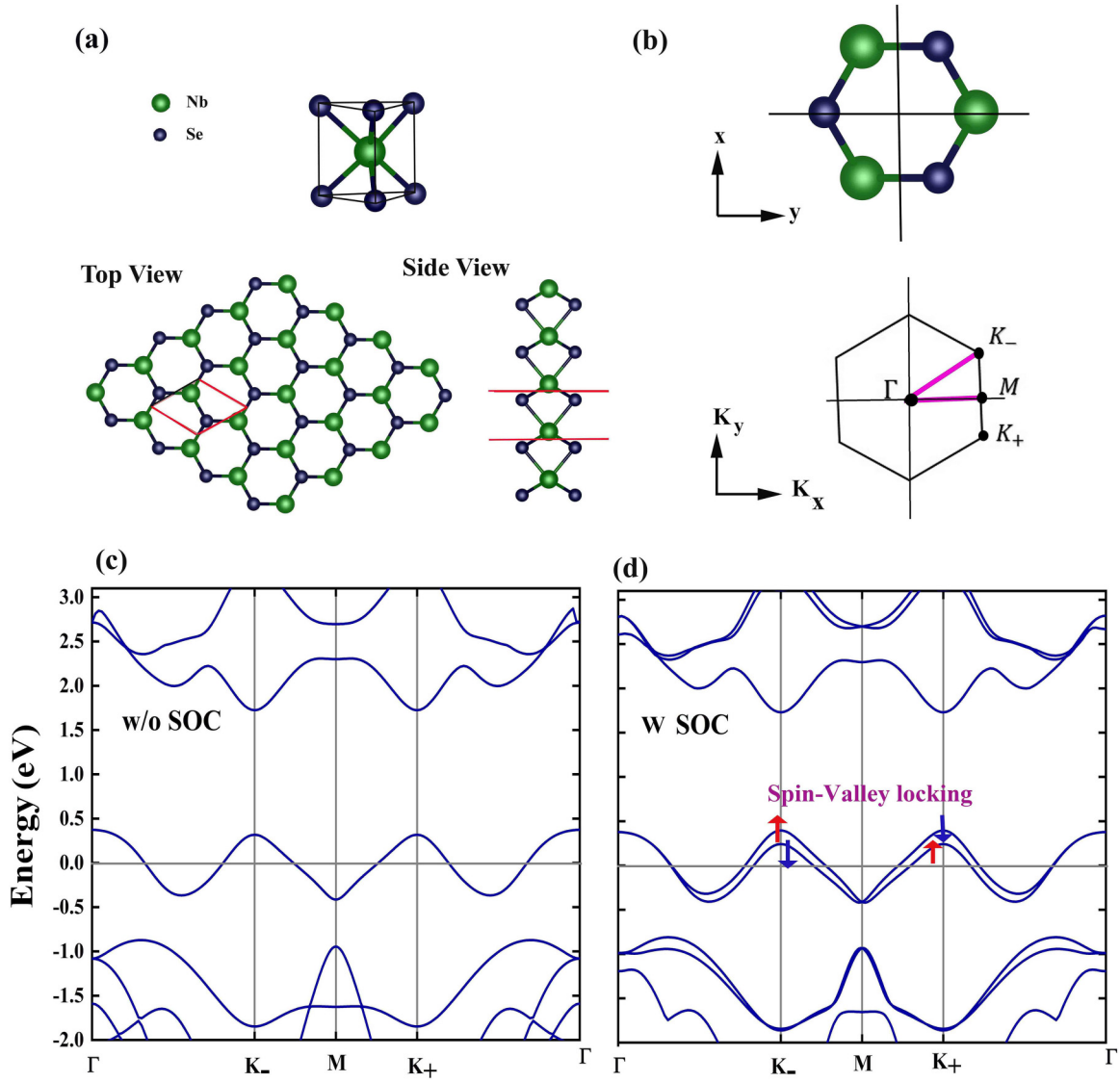

FIG. 2. (a) Crystal structure of the monolayer 2H-$NbSe_2$ with a trigonal prismatic structure. The single unit cell is depicted by the red rhombus in (a). (b) Arrangement of Se and Nb atoms (upper panel) and its relationship to 2D hexagonal first Brillouin zone along high-symmetry line (lower panel). Band structure of 2H-$NbSe_2$ monolayer without (c) and with (d) considering SOC.

results [88–90]. Each Nb atom is enclosed in a trigonal prismatic cage formed by the NN Se atoms. $NbSe_2$ monolayer has space group $P-6m2$ and point group D_{3h}, in which atomic arrangement is symmetric with respect to the y-z plane but not with respect to x-z plane, as shown in Fig. 2(b). Despite having out-of-plane mirror symmetry, the $NbSe_2$ monolayer suffers from a lack of inversion symmetry. Hence, the strong SOC field leads to a special type of SOC called Ising SOC [91–94]. It acts like a Zeeman field that pins the spin of electrons to the opposite out-of-plane directions for electrons with opposite momentum, unlike the Rashba effect in which the spin of the electrons is oriented in the direction of the plane [21–23,95].

Figure 2(c) shows the $NbSe_2$ monolayer band structure without considering SOI. The valence band crosses the Fermi level several times in the Brillouin zone, indicating that the material is a metal. The results are in good agreement with the images obtained from ARPES [24]. Although the shape of the band structure is almost identical to that of the monolayer MoS_2, because the Nb atom has one less d electron than Mo one, monolayer $NbSe_2$ exhibits metallic behavior. Considering the SOI, the valence band is split at the valleys as high as 154 meV. The splitting is caused by Zeeman SOC and is very significant in the valence band. Due to the presence of time-reversal symmetry and the highly delocalized nature of the electrons in the 4d-Nb orbital, the $NbSe_2$ monolayer is nonmagnetic.

To describe the band structure and the Ising SOC near the valleys, we take the model Hamiltonian proposed by Xiao *et al.* [22] for TMD monolayers as

$$H=\sum_{\mathbf{k},\tau=\pm1}\left[at(\tau k_x\sigma_x+\tau k_y\sigma_y)+\frac{\Delta}{2}\sigma_z-\lambda\tau\frac{\sigma_z-1}{2}s_z\right], \tag{5}$$

where $\tau=\pm1$ is the valley index, λ is half the spin splitting on top of the valence band caused by Ising SOC,

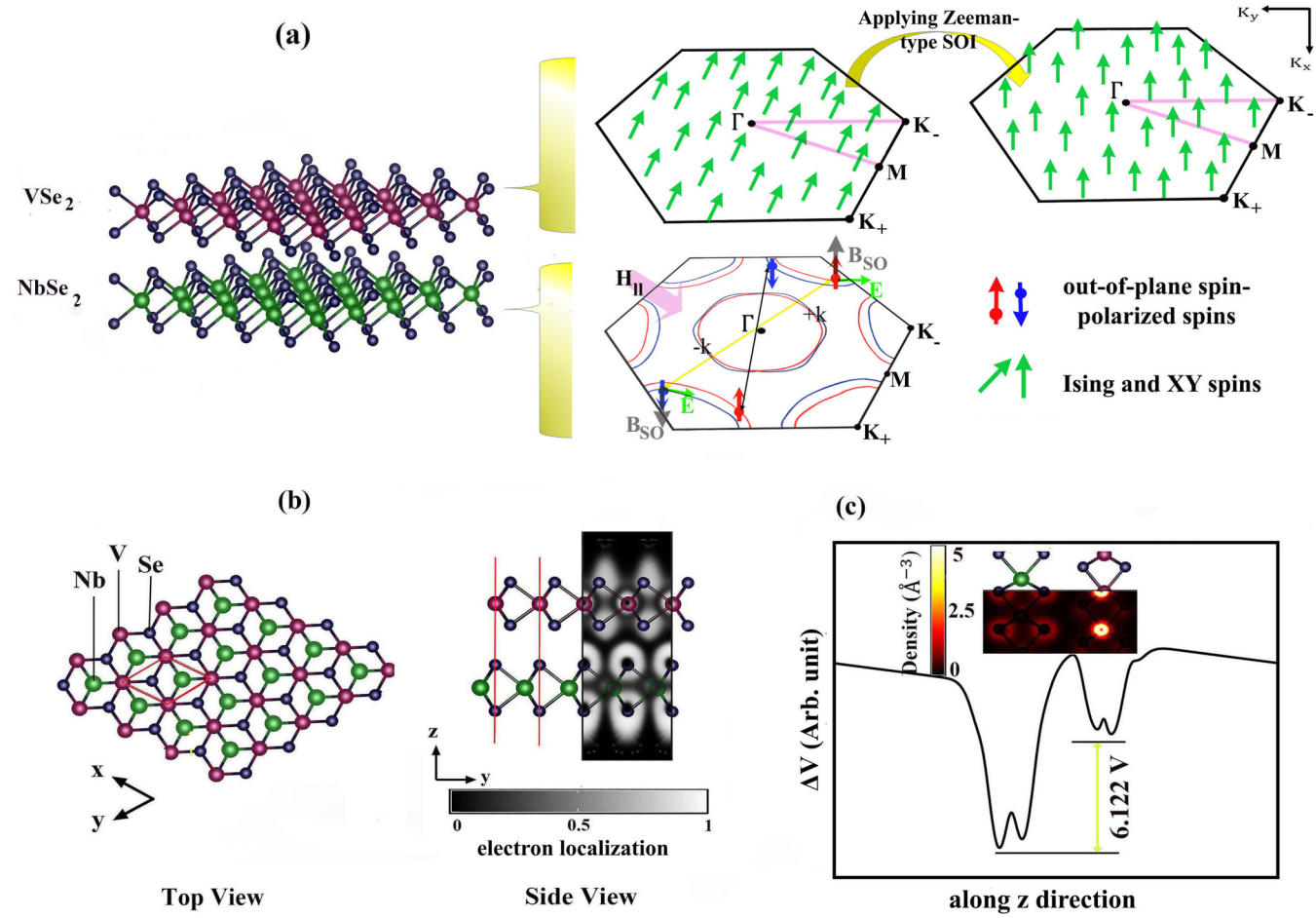

FIG. 3. (a) Magnetic van der Waals heterostructure made of VSe_2 and $NbSe_2$, providing XY/Ising magnet transition mediated by Zeeman-type SOI. The Fermi surface of VSe_2 monolayer in presence and absence of Zeeman-type SOI of $NbSe_2$ substrate with spin-split Fermi surfaces around $K_\pm$ valleys has been shown in (a). Spins of $NbSe_2$ substrate in $K_\pm$ valleys are aligned in the out-of-plane direction due to the effective magnetic field $B_{SOC} \propto \mathbf{E} \times \mathbf{k}$. Time-reversed spin pairs connected together by straight black and yellow lines in (a). (b) Top and side views of heterostructure $VSe_2/NbSe_2$ and ELF contour on the plane vertical to layer and crossing V, Nb, and Se atomic centers. (c) Electrostatic potential difference along z direction. The electron densities contoured by dark-orange-yellow maps on the layer plane through the bonding atoms are also shown in the inset of (c).

s_z is the Pauli matrix for a spin, and Δ is the energy gap. t is a hopping term, $k_{x(y)}$ denotes wave vector from the valleys, and σ_i stands for the Pauli matrix for two basis functions at two valleys, $\frac{1}{\sqrt{2}}(|d_{x^2-y^2}\rangle + i\tau|d_{xy}\rangle)$ for the valence band and $|d_{z^2}\rangle$ for the conduction band. By diagonalization of the Hamiltonian and expansion up to first order, energy eigenvalues for each spin channel around the valleys are obtained as

$$E_c^\sigma(k_x, k_y) = \frac{\Delta}{2} + \frac{a^2t^2k^2}{\Delta} + \frac{\lambda^2}{4\Delta}, \tag{6a}$$

$$E_V^\sigma(k_x, k_y) = -\frac{\Delta}{2} - \frac{a^2t^2k^2}{\Delta} + \sigma\lambda\tau - \frac{\lambda^2}{4\Delta}. \tag{6b}$$

where $\sigma = \uparrow (\downarrow)$ denotes spin up (down) and $E_{C(V)}$ is energy of the conduction (valence) band edge. It is clear from Eq. (2) that there is a band gap as high as Δ between the conduction and valence bands when SOI is ignored. The SOI has a dominant effect on the valence band, but its effect on the conduction band is negligible and is dependent on λ^2. In the K_+ valley, the spin-up band is 2λ above the spin-down band, while in the K_- valley the story is reversed. Hence, a spin-valley locking is observed in $NbSe_2$, which is similar to the MoS_2 monolayer [96–98]. However, the important difference is that the former is metal while the latter is a semiconductor.

Due to the antisymmetric form of SOI in 2H-$NbSe_2$ with in-plane inversion asymmetry, an effective magnetic field $B_{SOC} \propto \mathbf{E} \times \mathbf{k}$ pins the spin of electrons to the out-of-plane direction, where the crystal electric field $\mathbf{E}$ is restricted to point in plane [as shown in Fig. 3(a)]. So, energy splitting $g\mu_B B_{SOC}(\mathbf{k})$ occurs between the spins in each of the K_- and K_+ valleys. As a result, the time-reversed Cooper pair arises between electrons of two opposite spins and momentum in the Fermi surface around K_- and K_+ valleys, which are connected by straight black lines in Fig. 3(a). The Zeeman-type SOI forms intervalley Cooper pairs obeying the time-reversal symmetry, which have Fermi surfaces with almost the same radius and shape but opposite out-of-plane spin directions in two different valleys.

TABLE II. Structural parameters and magnetic moment of $NbSe_2/VSe_2$ heterostructure: Bond length of V (Nb)-Se and V-Nb, bond angle [$\theta_{V(Nb)-Se-V(Nb)}$], energy difference (E_{tot}), considering van der Waals interaction and spin polarization, and magnetic moment of V atom.

Structure	h (Å)	$d_{V\ (Nb)-Se}$ (Å)	d_{V-Nb} (Å)	$\theta_{V(Nb)-Se-V(Nb)}$	E_{tot} (meV)	m (μ_B/cell)
AA	3.408	2.53 (2.61)	6.60	86.5 (83.4)	113.94	0.92
AA′	2.98	2.54 (2.61)	6.51	86.4 (83.4)	20.02	0.92
AB	2.89	2.53 (2.60)	6.42	86.4 (83.4)	6.93	0.93
AB′	2.88	2.53 (2.61)	6.41	86.4 (83.3)	0	0.94

V. HETEROSTRUCTURE

A. Structural configuration

In this paper, we investigate the effect of Zeeman-SOI-mediated exchange interaction on the magnetic properties of a 2D XY ferromagnet 2H-VSe_2 across the vdW interface. Our paper demonstrates that 2H-$NbSe_2$ can serve as an ideal Zeeman SOI host material, which has fully out-of-plane spin-polarized electrons near E_F [schematically illustrated in Fig. 3(a)]. We show in the next section that the VSe_2 monolayer becomes an Ising ferromagnet with strong out-of-plane magnetic anisotropy upon neighboring metallic 2D $NbSe_2$, schematically shown in Fig. 3(a).

Therefore, we here examine the effect of Zeeman-type SOI in 2H-$NbSe_2$ on the magnetism of the 2D XY ferromagnet 2H-VSe_2 across the vdW interface. So, we considered a heterostructure consisting of 2H-$NbSe_2$ and 2H-VSe_2 monolayers with different configurations. To find the most stable configuration in the $NbSe_2/VSe_2$ heterostructure, four stacking patterns were considered: (i) V atoms on top of Nb ones (AA stack), (ii) Se atoms of VSe_2 monolayer on top of Nb atoms (AA stack), (iii) V atoms on top of hollow sites (center of the hexagon) of the $NbSe_2$ monolayer (AB stack), and, finally, (iv) Se atoms of VSe_2 on top of hollow sites of the $NbSe_2$ monolayer (AB stack).

The different optimized stacks considered in this paper are depicted in Fig. S3. The total energy of the optimized structures by taking into account vdW interaction and spin polarization is listed in Table II. The AB stack is the most stable configuration and AB and AA stacks are metastable. Results reveal that the heterostructure prefers a 1T shape configuration for bilayer arrangement, although each layer is in a 2H configuration. The vertical distance between layers is shorter in the AB stack and also the distance between Nb and V atoms is shorter too, so the interaction between layers is stronger in the AB stack, resulting in the stabilization of the AB atomic arrangement. Unlike vertical distance between layers and Nb-V distance, Nb-Se and V-Se bond lengths and the angle between TM-Se-TM are nearly independent of the stack, showing a weak influence of vdW interaction on the atomic arrangements of individual layers. In the following sections, we focus on the most stable stack AB [as shown in Fig. 3(b)] and present results for other stacks in supplementary information for comparison.

The ELF [Fig. 3(b)] reveals electron density localized mostly at Se and V atoms without electron gas localized in the interlayer region (ELF value is about 0), so the charge redistribution cannot be assigned for the creation of covalent bonds between two layers. There is a built-in potential with a height of 6.122 V between layers, leading to the induction of an electric field toward the VSe_2 sheet, as shown in Fig. 3(c). So, the net charge is transferred from the $NbSe_2$ to VSe_2 sheet and the electron density in the inset of Fig. 3(c) confirms this claim.

According to Fig. 4, the heterostructure has metallic behavior in the AB stack. By quenching the SOC, the spin splitting of the valence band in the VSe_2 ferromagnet is reduced upon contact with the $NbSe_2$ monolayer, and the Fermi level upshifts and crosses the minority spin of the valence band. Another important aspect is that the spin degeneracy is broken along the Γ-K-M direction due to time-reversal asymmetry, but spin-valley locking does not occur due to the absence of SOC. So the electron of the V^{4+} ion partially fills the spin-down valence band according to Hund's rule, resulting in a magnetic moment value to be half integer and smaller than 1 μ_B per V atom in pristine VSe_2, which is nearly independent of the stack (as shown in Table II).

B. Magnetic and valleytronic properties

After examining the structural characteristics of the heterostructure and recognizing the AB′ arrangement as the most stable atomic arrangement, we investigate the magnetic ground state of the heterostructure. For this purpose, we considered a rectangular superlattice consisting of 4 V, 4 Nb, and 16 Se atoms as the case of VSe_2. Three different spin arrangements (one FM and two AFM arrangements) were considered. The difference in the arrangement of antiferromagnets is in the spin orientation of the vanadium atoms. In the AFM1 arrangement, the vanadium atoms on a line in the y direction have the same spin orientation. In the AFM2 arrangement, vanadium atoms with the same y coordinate alternate their spin orientation between neighboring V atoms. In all considered AFM arrangements, there are four antiferromagnetic interactions between the nearest V atoms and two FM interactions. In contrast, there are four FM interactions between the NNN in the AFM1, while the number in the AFM2 configuration is 2.

Total energy of different spin arrangements shows that the ground state of the system is FM so the energy difference between the FM state and the AFM1 and AFM2 arrangements is equal to 97.6 meV/V and 82.02 meV/V, respectively. Therefore, the presence of the $NbSe_2$ substrate has no effect on the VSe_2 magnetic ground state, and the ferromagnetic order is still predominant.

In contrast, the $NbSe_2$ has led to a transition in the VSe_2 structure from an XY magnet to an Ising magnet with an out-off-plane easy axis. Using the spin Hamiltonian presented in Eq. (1), J_1 and J_2, and D are equal to 20.51 meV, −7.79 meV, and 1.17 meV, respectively. In comparison with freestanding VSe_2, J_1 and J_2 are reduced four and two times, whereas D is

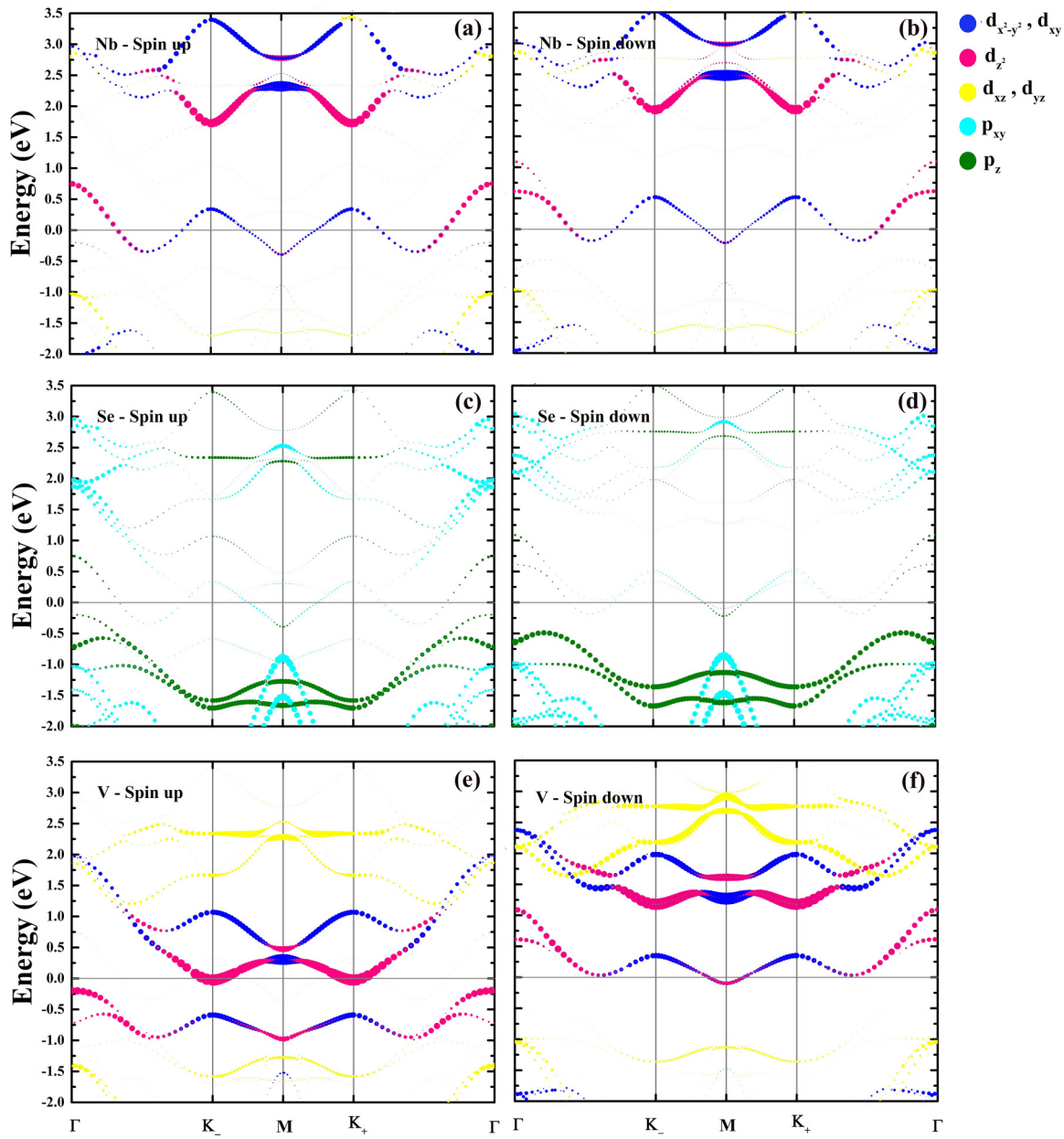

FIG. 4. (a)–(f) Band structure of heterostructure $VSe_2/NbSe_2$ projected onto atomic orbitals in spin-up (left panels) and -down (right panels) channels without considering spin-orbit interaction. The size of the circles illustrates the projected weight of the orbitals. The Fermi level is set to be zero energy.

doubled. So, the MAE of the structure in the presence of the $NbSe_2$ and the SOI indicates that the preferred spin orientation is out of plane. The MAE achieved in the heterostructure is comparable with 1.37 meV/cell, 2.76 meV/cell reported for CrI_3 [99], and $FeGeTe_2$ [100], respectively. Indeed, strong SOC in $NbSe_2$ controls the magnetic properties of VSe_2. According to the orbital band structure shown in Fig. 5, it is clear that in addition to the spin down, the spin up of all *d* orbitals also participates in CBM by applying Zeeman-type SOI of the substrate. Therefore, according to the above relations Figs. 3(a) and 3(b), a nonvanishing term related to $\langle d^{(+)}_{x^2-y^2}|L_z|d^{(+)}_{xy}\rangle$ with a positive sign is added to the MAE and the phase transition from the XY model to the Ising model occurs. So, due to the unique interplay between ferromagnetism and Zeeman SOI mediated by the 2D $NbSe_2$ substrate, strong magnetic anisotropy was induced normal to the VSe_2 film, which holds great promise for faster and smaller magnetic bits in the future to be used in storage applications such as high-density nonvolatile memory and logic circuits using current-induced magnetization switching [85,86].

According to the dominant contribution of the $|d_{z^2}\rangle$ state at the VBM of the V atom after the presence of the $NbSe_2$ substrate, the orbital magnetic moment at the V sites is close to zero. It has already been shown experimentally in Ref. [37] that integrated intensity of the X-ray magnetic circular dichroism signals of V_5Se_8 over L_2 and L_3 edges is negligible. So, we can claim that the transition to strong out-of-plane

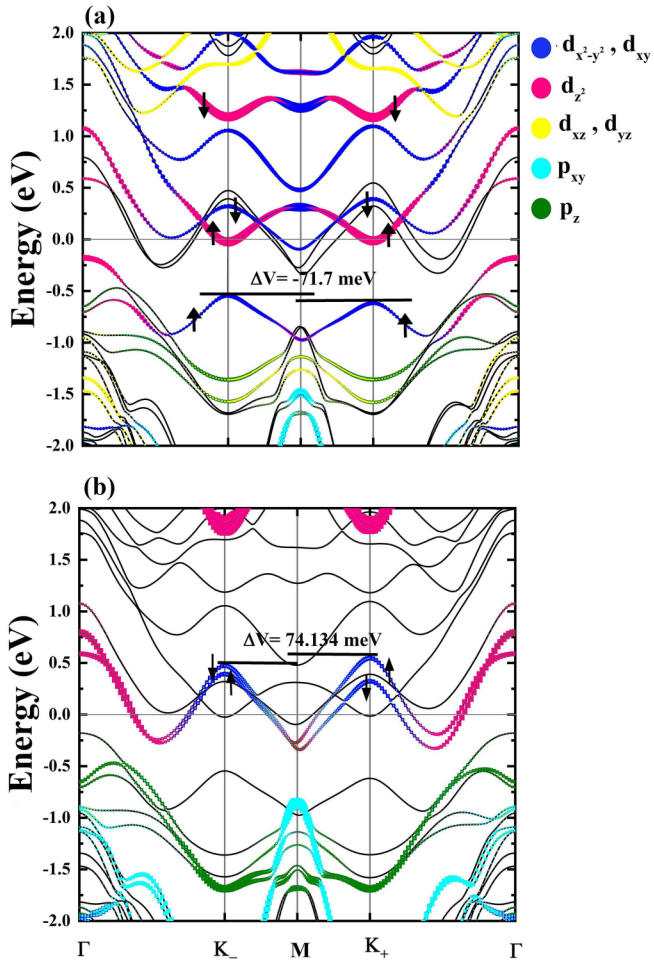

FIG. 5. Band structure of heterostructure $VSe_2/NbSe_2$ projected on (a) V and (b) Nb atomic orbitals, considering both the ferromagnetism and SOC effect. The up (down) black arrows represent the spin-up (spin-down) channel near the Fermi level. The size of the circles illustrates the projected weight of the orbitals. The Fermi level is set to be zero energy.

magnetic anisotropy in $NbSe_2/VSe_2$ heterostructure is not due to the crystalline anisotropy induced by the built-in electric field or interface stress but is due to the Zeeman-type SOI in $NbSe_2$ which has not associated with the orbital magnetic moment.

Interestingly, when the Zeeman-type SOI of $NbSe_2$ is included, the valley polarization of the VSe_2 system is significantly reversed [as shown in Fig. 5(a)], providing the possibilities to manipulate the valley degree of freedom by means of a type of interface magnetic proximity effect mediated by Zeeman SOI. When the polarity of the polarization is reversed, charges accumulate on the other side of the sample due to the negative Berry curvature, resulting in the transverse voltage with opposite signs.

Figure 5(b) shows the magnitude of spin splitting energy is different and opposite in sign at K_+ and K_- valleys because of time-reversal asymmetry, and it is expected that threefold symmetry is distorted in the first Brillouin zone [101]. A large valley splitting has appeared in this layer, equal to 74.13 meV. Due to the unequal number of up- and down-spin electrons below the Fermi level, a ferromagnetic ground state with spontaneous spin polarization is formed in $NbSe_2$. In such a case, we expect a nonzero anomalous Hall conductance, which is due to the incomplete cancellation of the Berry curve below the Fermi level.

In the following, to describe edge-bands of 2H−VSe_2 monolayer near the K_- and K_+ valleys, we propose a low-energy effective Hamiltonian in momentum space with the structure [61,102]

$$H = \hbar v_f(\tau q_x\hat{\sigma}_x + q_y\hat{\sigma}_y) + \frac{\Delta}{2}\hat{\sigma}_z + \varepsilon I + \tau\left(\lambda\frac{(1-\hat{\sigma}_z)}{2} + \lambda'\frac{(1+\hat{\sigma}_z)}{2}\right)\hat{S}_z - \left(m_c\frac{(1+\hat{\sigma}_z)}{2} + m_v\frac{(1-\hat{\sigma}_z)}{2}\right)\hat{S}_z, \tag{7}$$

where $\sigma_{x,y,z}$ denotes the Pauli matrices of the sublattice pseudospin for two basis functions at K_- and K_+ valleys: $|\psi_\tau^c\rangle = |d_{z^2}\rangle$ and $|\psi_\tau^v\rangle = (|d_{x^2-y^2}\rangle + i\tau|d_{xy}\rangle/\sqrt{2})$, and $\hat{S}_z$ is the spin matrix for the z component of spin s_z. λ and λ' indicate SOC spin splitting of valence and conduction bands, respectively; and m_v and m_c describe the exchange spin splitting in the valence and conduction band edges, respectively. Δ, ε, and v_f are band gap, correction energy, and Fermi velocity, respectively.

Edge bands of DFT energy dispersion near the K_- and K_+ valleys fitted by the two-band $k\cdot p$ model using the parameters listed in Table III, which are in agreement with the parameters reported in previous studies [61,103]. By solving the eigenvalue equation as $H\,|u^{\pm}_{(\tau,s_z)}\rangle = \epsilon^{\pm}_{(\tau,s_z)}\,|u^{\pm}_{(\tau,s_z)}\rangle$, we obtained the energy dispersion of VSe_2 monolayer (as shown in Fig. 6) in the presence and absence of Zeeman-type SOI. The band dispersion obtained through the $k\cdot p$ model is in good agreement with the DFT band structure near Dirac points (Fig. 1). So, it can be concluded that the $k\cdot p$ model provides a suitable model for describing the valleytronic properties of 2H−VSe_2.

It is clear that by applying the Zeeman-type SOI to VSe_2 monolayer, all the bands have shifted to lower energies, so the valence band has completely cut off the Fermi energy. Also, according to Table III, the values of the spin splitting parameters caused by the exchange field and SOC (m_v, m_c,

TABLE III. The $k\cdot p$ parameters obtained by fitting the DFT band structures for the 2H-VSe_2 layer in monolayer/heterostructure: Spin splitting caused by SOC effect in the valence band (λ) and conduction band (λ'), spin splitting caused by intrinsic magnetic exchange field in the valence band (m_v) and conduction band (m_c), band gap at the $K_\pm$ valleys (Δ), correction energy relative to the Fermi level (ε).

2H-VSe_2	m_v (meV)	m_c (meV)	λ (meV)	λ' (meV)	Δ (meV)	ϵ (meV)
Monolayer	455.35	567.25	−37.9	8.99	847.4	719.25
Heterostructure	504.3	601.55	35.85	−4.2	659.6	251.55

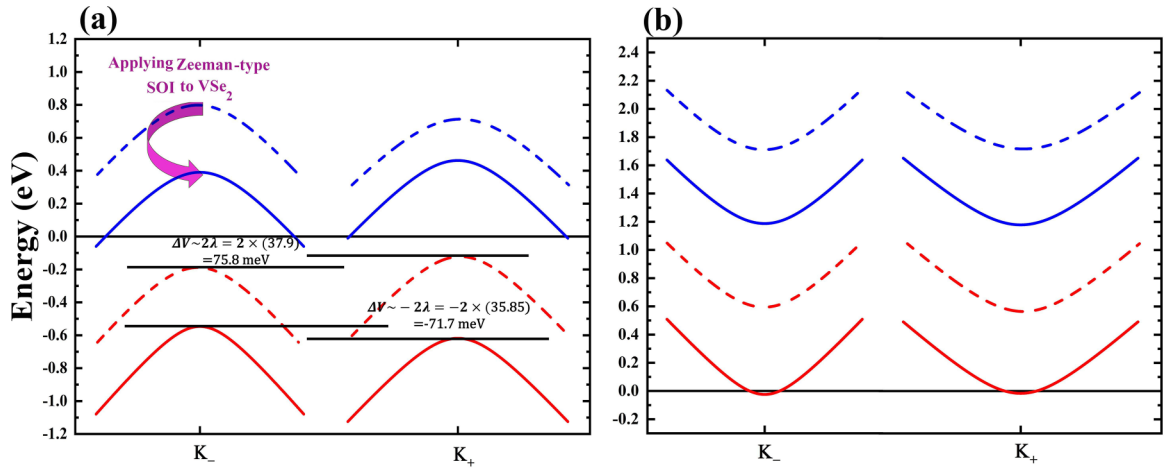

FIG. 6. The electronic (a) valence and (b) conduction bands obtained through the $\boldsymbol{k}\cdot\boldsymbol{p}$ model in VSe_2 monolayer near the K_- and K_+ valleys in the presence (solid lines) and absence (dashed lines) of Zeeman-type SOI of $NbSe_2$ substrate.

λ, and λ') have changed significantly in the presence of the $NbSe_2$ substrate, and directions of SOC parameters (λ and λ') have changed, which directly causes the reversal of polarization in valence and conductance bands [$\Delta V \backsimeq 2\lambda$, as shown in Fig. 6(a)].

Note that these results may be subject to change by taking into account the lattice-mismatch strain ($\sim$3%) between the substrate and the VSe_2 monolayer. But our results in Ref. [104] as well as the results reported in Refs. [43,80] show that the variation of the in-plane MAE and J_1 is not sensitive to the applied strain in range of -1.5% to $+3\%$ in V-based TMD materials, so we did not consider lattice-mismatch strain in our calculations.

VI. CONCLUSION

To summarize, first-principles calculations were performed to study the magnetic proximity effect, Zeeman-type SOI, at the vdW interface of $NbSe_2/VSe_2$ heterostructure. The results obtained in the present paper provide a route to manipulate the valleytronic and magnetic properties of recently synthesized ferromagnet: 2H-VSe_2 monolayer. By examining the structural and magnetic properties of the four different stackings for arrangement of atoms in the $NbSe_2/VSe_2$ heterostructure and finally focusing on the most stable configuration, we found that the $NbSe_2$ substrate has no effect on the VSe_2 magnetic ground state and the FM order is still predominant. In contrast, the $NbSe_2$ leads to strong out-of-plane magnetic anisotropy in VSe_2. The transition of XY to Ising ferromagnetism at the interface of $NbSe_2/VSe_2$ heterostructure offers a great opportunity for realizing next-generation high-density nonvolatile memory.

ACKNOWLEDGMENTS

We are thankful to the Research Council of the University of Guilan for partial support of this research. M.B.T. wishes to acknowledge the support of the Iran National Science Foundation (INSF) under Grant No. 98021284. The authors declare that they have no conflict of interest.

[1] N. D. Mermin and H. Wagner, Absence of Ferromagnetism or Antiferromagnetism in One-or Two-Dimensional Isotropic Heisenberg Models, Phys. Rev. Lett. **17**, 1133 (1966).

[2] C. Gong, L. Li, Z. Li, H. Ji, A. Stern, Y. Xia, T. Cao, W. Bao, C. Wang, Y. Wang *et al.*, Discovery of intrinsic ferromagnetism in two-dimensional van der Waals crystals, Nature (London) **546**, 265 (2017).

[3] W. Xing, Y. Chen, P. M. Odenthal, X. Zhang, W. Yuan, T. Su, Q. Song, T. Wang, J. Zhong, S. Jia *et al.*, Electric field effect in multilayer $Cr_2Ge_2Te_6$: A ferromagnetic 2D material, 2D Mater. **4**, 024009 (2017).

[4] M. A. McGuire, G. Clark, S. KC, W. M. Chance, G. E. Jellison Jr, V. R. Cooper, X. Xu, and B. C. Sales, Magnetic behavior and spin-lattice coupling in cleavable van der Waals layered $CrCl_3$ crystals, Phys. Rev. Mater. **1**, 014001 (2017).

[5] J. M. Kosterlitz and D. J. Thouless, Ordering, metastability and phase transitions in two-dimensional systems, J. Phys. C **6**, 1181 (1973).

[6] L. Onsager, Crystal statistics. I. A two-dimensional model with an order-disorder transition, Phys. Rev. **65**, 117 (1944).

[7] B. Huang, G. Clark, E. Navarro-Moratalla, D. R. Klein, R. Cheng, K. L. Seyler, D. Zhong, E. Schmidgall, M. A. McGuire, D. H. Cobden *et al.*, Layer-dependent ferromagnetism in a van der Waals crystal down to the monolayer limit, Nature (London) **546**, 270 (2017).

[8] Y.-J. Lin, K. Jiménez-García, and I. B. Spielman, Spin–orbit-coupled Bose-Einstein condensates, Nature (London) **471**, 83 (2011).

[9] S. Murakami, N. Nagaosa, and S.-C. Zhang, Dissipationless quantum spin current at room temperature, Science **301**, 1348 (2003).

[10] J. P. Lu, J.-B. Yau, S. P. Shukla, M. Shayegan, L. Wissinger, U. Rössler, and R. Winkler, Tunable Spin-Splitting and Spin-Resolved Ballistic Transport in GaAs/AlGaAs Two-Dimensional Holes, Phys. Rev. Lett. **81**, 1282 (1998).

[11] A. M. Clogston, Upper Limit for the Critical Field in Hard Superconductors, Phys. Rev. Lett. **9**, 266 (1962).

[12] B. Chandrasekhar, A note on the maximum critical field of high-field superconductors, Appl. Phys. Lett. **1**, 7 (1962).

[13] A. A. Abrikosov, L. P. Gorkov, I. E. Dzyaloshinski, and R. A. Silverman, *Methods of Quantum Field Theory in Statistical Physics*, Dover Books on Physics (Dover Publications, 2012), p. 48.

[14] N. Werthamer, E. Helfand, and P. Hohenberg, Temperature and purity dependence of the superconducting critical field, H_{c2}. III Electron spin and spin-orbit effects, Phys. Rev. **147**, 295 (1966).

[15] Y. Liu, Z. Wang, X. Zhang, C. Liu, Y. Liu, Z. Zhou, J. Wang, Q. Wang, Y. Liu, C. Xi *et al.*, Interface-Induced Zeeman-Protected Superconductivity in Ultrathin Crystalline Lead Films, Phys. Rev. X **8**, 021002 (2018).

[16] P. A. Frigeri, D. F. Agterberg, and M. Sigrist, Spin susceptibility in superconductors without inversion symmetry, New J. Phys. **6**, 115 (2004).

[17] E. I. Rashba, Properties of semiconductors with an extremum loop. I. Cyclotron and combinational resonance in a magnetic field perpendicular to the plane of the loop, Sov. Phys. Solid State **2**, 1109 (1960).

[18] Y. A. Bychkov and E. I. Rashba, Oscillatory effects and the magnetic susceptibility of carriers in inversion layers, J. Phys. C **17**, 6039 (1984).

[19] J. Lu, O. Zheliuk, I. Leermakers, N. F. Yuan, U. Zeitler, K. T. Law, and J. Ye, Evidence for two-dimensional Ising superconductivity in gated MoS_2, Science **350**, 1353 (2015).

[20] Y. Saito, Y. Nakamura, M. S. Bahramy, Y. Kohama, J. Ye, Y. Kasahara, Y. Nakagawa, M. Onga, M. Tokunaga, T. Nojima *et al.*, Superconductivity protected by spin–valley locking in ion-gated MoS_2, Nat. Phys. **12**, 144 (2016).

[21] Z. Y. Zhu, Y. C. Cheng, and U. Schwingenschlögl, Giant spin-orbit-induced spin splitting in two-dimensional transition-metal dichalcogenide semiconductors, Phys. Rev. B **84**, 153402 (2011).

[22] D. Xiao, G.-B. Liu, W. Feng, X. Xu, and W. Yao, Coupled Spin and Valley Physics in Monolayers of MoS_2 and other Group-VI Dichalcogenides, Phys. Rev. Lett. **108**, 196802 (2012).

[23] X. Xu, W. Yao, D. Xiao, and T. F. Heinz, Spin and pseudospins in layered transition metal dichalcogenides, Nat. Phys. **10**, 343 (2014).

[24] Y. Nakata, K. Sugawara, S. Ichinokura, Y. Okada, T. Hitosugi, T. Koretsune, K. Ueno, S. Hasegawa, T. Takahashi, and T. Sato, Anisotropic band splitting in monolayer $NbSe_2$: Implications for superconductivity and charge density wave, npj 2D Mater. Appl. **2**, 12 (2018).

[25] W.-Y. He, B. T. Zhou, J. J. He, N. F. Yuan, T. Zhang, and K. T. Law, Magnetic field driven nodal topological superconductivity in monolayer transition metal dichalcogenides, Commun. Phys. **1**, 40 (2018).

[26] Y. Saito, T. Nojima, and Y. Iwasa, Highly crystalline 2D superconductors, Nat. Rev. Mater. **2**, 16094 (2016).

[27] Q. Cui, J. Liang, B. Yang, Z. Wang, P. Li, P. Cui, and H. Yang, Giant enhancement of perpendicular magnetic anisotropy and induced quantum anomalous Hall effect in graphene/NiI_2 heterostructures via tuning the van der Waals interlayer distance, Phys. Rev. B **101**, 214439 (2020).

[28] D. Zhong, K. L. Seyler, X. Linpeng, R. Cheng, N. Sivadas, B. Huang, E. Schmidgall, T. Taniguchi, K. Watanabe, M. A. McGuire *et al.*, Van der Waals engineering of ferromagnetic semiconductor heterostructures for spin and valleytronics, Sci. Adv. **3**, e1603113 (2017).

[29] W. Sun, W. Wang, D. Chen, Z. Cheng, and Y. Wang, Valence mediated tunable magnetism and electronic properties by ferroelectric polarization switching in 2D FeI_a22/In_2Se_3 van der Waals heterostructures, Nanoscale **11**, 9931 (2019).

[30] L. Ciorciaro, M. Kroner, K. Watanabe, T. Taniguchi, and A. Imamoglu, Observation of Magnetic Proximity Effect Using Resonant Optical Spectroscopy of an Electrically Tunable $MoSe_2/CrBr_3$ Heterostructure, Phys. Rev. Lett. **124**, 197401 (2020).

[31] J. C. Egues, G. Burkard, and D. Loss, Rashba spin-orbit interaction and shot noise for spin-polarized and entangled electrons, Phys. Rev. Lett. **89**, 176401 (2002).

[32] E. I. Rashba and A. L. Efros, Orbital Mechanisms of Electron-Spin Manipulation by an Electric Field, Phys. Rev. Lett. **91**, 126405 (2003).

[33] C. Weeks, J. Hu, J. Alicea, M. Franz, and R. Wu, Engineering a Robust Quantum Spin Hall State in Graphene Via Adatom Deposition, Phys. Rev. X **1**, 021001 (2011).

[34] T. Wakamura, F. Reale, P. Palczynski, S. Guéron, C. Mattevi, and H. Bouchiat, Strong Anisotropic Spin-Orbit Interaction Induced in Graphene by Monolayer WS_2, Phys. Rev. Lett. **120**, 106802 (2018).

[35] L. A. Benítez, J. F. Sierra, W. Savero Torres, A. Arrighi, F. Bonell, M. V. Costache, and S. O. Valenzuela, Strongly anisotropic spin relaxation in graphene–transition metal dichalcogenide heterostructures at room temperature, Nat. Phys. **14**, 303 (2018).

[36] X.-J. Dong, J.-Y. You, Z. Zhang, B. Gu, and G. Su, Great enhancement of Curie temperature and magnetic anisotropy in two-dimensional van der Waals magnetic semiconductor heterostructures, Phys. Rev. B **102**, 144443 (2020).

[37] H. Matsuoka, S. E. Barnes, J. Ieda, S. Maekawa, M. S. Bahramy, B. K. Saika, Y. Takeda, H. Wadati, Y. Wang, S. Yoshida *et al.*, Spin–orbit-induced Ising ferromagnetism at a van der Waals interface, Nano Lett. **21**, 1807 (2021).

[38] X. Wang, D. Li, Z. Li, C. Wu, C.-M. Che, G. Chen, and X. Cui, Ferromagnetism in 2D vanadium diselenide, ACS Nano **15**, 16236 (2021).

[39] M. Bonilla, S. Kolekar, Y. Ma, H. C. Diaz, V. Kalappattil, R. Das, T. Eggers, H. R. Gutierrez, M.-H. Phan, and M. Batzill, Strong room-temperature ferromagnetism in VSe_2 monolayers on van der Waals substrates, Nat. Nanotechnol. **13**, 289 (2018).

[40] G. Duvjir, B. K. Choi, I. Jang, S. Ulstrup, S. Kang, T. Thi Ly, S. Kim, Y. H. Choi, C. Jozwiak, A. Bostwick *et al.*, Emergence of a Metal–insulator Transition and High-Temperature Charge-Density Waves in VSe_2 at the Monolayer Limit, Nano Lett. **18**, 5432 (2018).

[41] P. Chen, W. W. Pai, Y.-H. Chan, V. Madhavan, M.-Y. Chou, S.-K. Mo, A.-V. Fedorov, and T.-C. Chiang, Unique Gap Structure and Symmetry of the Charge Density Wave in Single-Layer VSe_2, Phys. Rev. Lett. **121**, 196402 (2018).

[42] J. Liu, W.-J. Hou, C. Cheng, H.-X. Fu, J.-T. Sun, and S. Meng, Intrinsic valley polarization of magnetic VSe_2 monolayers, J. Phys.: Condens. Matter **29**, 255501 (2017).

[43] S. Feng and W. Mi, Strain and interlayer coupling tailored magnetic properties and valley splitting in layered ferrovalley 2H-VSe_2, Appl. Surf. Sci. **458**, 191 (2018).
[44] S.-i. Iwasaki, Perpendicular magnetic recording-its development and realization, Proc. Jpn. Acad., Ser. B **85**, 37 (2009).
[45] N. F. Mott, Electrons in transition metals, Adv. Phys. **13**, 325 (1964).
[46] S. I. Kiselev, J. Sankey, I. Krivorotov, N. Emley, R. Schoelkopf, R. Buhrman, and D. Ralph, Microwave oscillations of a nanomagnet driven by a spin-polarized current, Nature (London) **425**, 380 (2003).
[47] G. Kresse and D. Joubert, From ultrasoft pseudopotentials to the projector augmented-wave method, Phys. Rev. B **59**, 1758 (1999).
[48] J. P. Perdew, K. Burke, and M. Ernzerhof, Generalized Gradient Approximation Made Simple, Phys. Rev. Lett. **77**, 3865 (1996).
[49] G. Kresse and J. Furthmüller, Efficient iterative schemes for ab initio total-energy calculations using a plane-wave basis set, Phys. Rev. B **54**, 11169 (1996).
[50] H. J. Monkhorst and J. D. Pack, Special points for Brillouin-zone integrations, Phys. Rev. B **13**, 5188 (1976).
[51] S. Grimme, Semiempirical GGA-type density functional constructed with a long-range dispersion correction, J. Comput. Chem. **27**, 1787 (2006).
[52] S. L. Dudarev, G. A. Botton, S. Y. Savrasov, C. J. Humphreys, and A. P. Sutton, Electron-energy-loss spectra and the structural stability of nickel oxide: An LSDA+U study, Phys. Rev. B **57**, 1505 (1998).
[53] D. Hobbs, G. Kresse, and J. Hafner, Fully unconstrained noncollinear magnetism within the projector augmented-wave method, Phys. Rev. B **62**, 11556 (2000).
[54] R. Chua, J. Yang, X. He, X. Yu, W. Yu, F. Bussolotti, P. K. J. Wong, K. P. Loh, M. B. Breese, K. E. J. Goh *et al.*, Can reconstructed se-deficient line defects in monolayer VSe_2 induce magnetism? Adv. Mater. **32**, 2000693 (2020).
[55] A. Feroze, H. R. Na, Y. C. Park, J.-H. Jun, M.-H. Jung, J.-H. Lee, J.-H. Kim, M.-J. Seong, S. Hong, S.-H. Chun *et al.*, In-depth structural characterization of 1T-VSe_2 single crystals grown by chemical vapor transport, Cryst. Growth Des. **20**, 2860 (2020).
[56] H.-R. Fuh, B. Yan, S.-C. Wu, C. Felser, and C.-R. Chang, Metal-insulator transition and the anomalous Hall effect in the layered magnetic materials VS_2 and VSe_2, New J. Phys. **18**, 113038 (2016).
[57] W.-F. Li, C. Fang, and M. A. van Huis, Strong spin-orbit splitting and magnetism of point defect states in monolayer WS_2, Phys. Rev. B **94**, 195425 (2016).
[58] H. Schmidt, F. Giustiniano, and G. Eda, Electronic transport properties of transition metal dichalcogenide field-effect devices: Surface and interface effects, Chem. Soc. Rev. **44**, 7715 (2015).
[59] C. Lei, X. Xu, T. Zhang, B. Huang, Y. Dai, and Y. Ma, Nonvolatile controlling valleytronics by ferroelectricity in 2H-VSe_2/SC_2CO_2 van der Waals heterostructure, J. Phys. Chem. C **125**, 2802 (2021).
[60] J. Wang, Z. Luo, X. Zhang, X. Zhang, J. Shi, T. Cao, and X. Fan, Single transition metal atom anchored on VSe_2 as electrocatalyst for nitrogen reduction reaction, Appl. Surf. Sci. **580**, 152272 (2022).
[61] W.-Y. Tong, S.-J. Gong, X. Wan, and C.-G. Duan, Concepts of ferrovalley material and anomalous valley Hall effect, Nat. Commun. **7**, 13612 (2016).
[62] H.-R. Fuh, C.-R. Chang, Y.-K. Wang, R. F. Evans, R. W. Chantrell, and H.-T. Jeng, Newtype single-layer magnetic semiconductor in transition-metal dichalcogenides VX_2 (X = S, Se and Te), Sci. Rep. **6**, 32625 (2016).
[63] A. A. Wasey, S. Chakrabarty, and G. Das, Quantum size effects in layered VX_2 (X = S, Se and Te) materials: Manifestation of metal to semimetal or semiconductor transition, J. Appl. Phys. **117**, 064313 (2015).
[64] A. Bafekry, M. Yagmurcukardes, B. Akgenc, M. Ghergherehchi, and C. V. Nguyen, Van der Waals heterostructures of MoS_2 and Janus MoSSe monolayers on graphitic boron-carbon-nitride (BC_3, C_3N, C_3N_4 and C_4N_3) nanosheets: A first-principles study, J. Phys. D **53**, 355106 (2020).
[65] G.-B. Liu, D. Xiao, Y. Yao, X. Xu, and W. Yao, Electronic structures and theoretical modelling of two-dimensional group-VIB transition metal dichalcogenides, Chem. Soc. Rev. **44**, 2643 (2015).
[66] See Supplemental Material at http://link.aps.org/supplemental/10.1103/PhysRevB.108.024427, for which consists of the spin-polarized band structure of the VSe_2 monolayer projected onto atomic orbitals, three magnetic configurations of the VSe_2 monolayer, and atomic configuration models of AA, AA′, AB, and AB′ in $VSe_2/NbSe_2$ heterostructure stacking structures.
[67] S. Guddala, Y. Kawaguchi, F. Komissarenko, S. Kiriushechkina, A. Vakulenko, K. Chen, A. Alù, V. M. Menon, and A. B. Khanikaev, All-optical nonreciprocity due to valley polarization pumping in transition metal dichalcogenides, Nat. Commun. **12**, 3746 (2021).
[68] C. Li, S.-C. Hsu, J.-X. Lin, J.-Y. Chen, K.-C. Chuang, Y.-P. Chang, H.-S. Hsu, C.-H. Chen, T.-S. Lin, and Y.-H. Liu, Giant zeeman splitting for monolayer nanosheets at room temperature, J. Am. Chem. Soc. **142**, 20616 (2020).
[69] Y. Wu, C. Shen, Q. Tan, J. Shi, X. Liu, Z. Wu, J. Zhang, P. Tan, and H. Zheng, Valley zeeman splitting of monolayer MoS_2 probed by low-field magnetic circular dichroism spectroscopy at room temperature, Appl. Phys. Lett. **112**, 153105 (2018).
[70] S. Owerre, A first theoretical realization of honeycomb topological magnon insulator, J. Phys.: Condens. Matter **28**, 386001 (2016).
[71] L. Chen, J.-H. Chung, B. Gao, T. Chen, M. B. Stone, A. I. Kolesnikov, Q. Huang, and P. Dai, Topological Spin Excitations in Honeycomb Ferromagnet CrI_3, Phys. Rev. X **8**, 041028 (2018).
[72] M. Esters, R. G. Hennig, and D. C. Johnson, Dynamic instabilities in strongly correlated VSe_2 monolayers and bilayers, Phys. Rev. B **96**, 235147 (2017).
[73] G. V. Pushkarev, V. G. Mazurenko, V. V. Mazurenko, and D. W. Boukhvalov, Structural phase transitions in VSe_2: Energetics, electronic structure and magnetism, Phys. Chem. Chem. Phys. **21**, 22647 (2019).
[74] Y. Ma, Y. Dai, M. Guo, C. Niu, Y. Zhu, and B. Huang, Evidence of the existence of magnetism in pristine VX2

monolayers (X = S, Se) and their strain-induced tunable magnetic properties, ACS Nano **6**, 1695 (2012).

[75] Z. Tang, Y. Chen, Y. Zheng, and X. Luo, Strain engineering magnetocrystalline anisotropy in strongly correlated VTe_2 with room-temperature ferromagnetism, Phys. Rev. B **105**, 214403 (2022).

[76] S.-C. Lee, K.-S. Kim, S.-H. Lee, U.-H. Pi, K. Kim, Y. Jang, and U.-I. Chung, Effect of Fe-O distance on magnetocrystalline anisotropy energy at the Fe/MgO (001) interface, J. Appl. Phys. **113**, 023914 (2013).

[77] D.-s. Wang, R. Wu, and A. J. Freeman, First-principles theory of surface magnetocrystalline anisotropy and the diatomic-pair model, Phys. Rev. B **47**, 14932 (1993).

[78] L. Ke, B. N. Harmon, and M. J. Kramer, Electronic structure and magnetic properties in T_2AlB_2 (T = Fe, Mn, Cr, Co, and Ni) and their alloys, Phys. Rev. B **95**, 104427 (2017).

[79] L. Ke, M. van Schilfgaarde, and V. Antropov, Spin excitations in $K_2Fe_{4+x}Se_5$: Linear response approach, Phys. Rev. B **86**, 020402(R) (2012).

[80] C. Wang and Y. An, Effects of strain and stacking patterns on the electronic structure, valley polarization and magnetocrystalline anisotropy of layered VTe_2, Appl. Surf. Sci. **538**, 148098 (2021).

[81] A. Kabiraj, T. Jain, and S. Mahapatra, Massive monte carlo simulations-guided interpretable learning of two-dimensional curie temperature, Patterns **3**, 100625 (2022).

[82] N. Guo, X. Fan, Z. Chen, Z. Luo, Y. Hu, Y. An, D. Yang, and S. Ma, Electronic and magnetic properties of group-V TMDs monolayers with defects: A first-principles study, Comput. Mater. Sci. **176**, 109540 (2020).

[83] Y. Wu, J. Li, and Y. Liu, Two-dimensional chalcogenide-based ferromagnetic semiconductors, J. Phys.: Condens. Matter **35**, 083002 (2022).

[84] S. Ikeda, K. Miura, H. Yamamoto, K. Mizunuma, H. Gan, M. Endo, S. Kanai, J. Hayakawa, F. Matsukura, and H. Ohno, A perpendicular-anisotropy CoFeB-MgO magnetic tunnel junction, Nat. Mater. **9**, 721 (2010).

[85] S. Mangin, D. Ravelosona, J. Katine, M. Carey, B. Terris, and E. E. Fullerton, Current-induced magnetization reversal in nanopillars with perpendicular anisotropy, Nat. Mater. **5**, 210 (2006).

[86] H. Meng and J.-P. Wang, Spin transfer in nanomagnetic devices with perpendicular anisotropy, Appl. Phys. Lett. **88**, 172506 (2006).

[87] T. Kishi, H. Yoda, T. Kai, T. Nagase, E. Kitagawa, M. Yoshikawa, K. Nishiyama, T. Daibou, M. Nagamine, M. Amano *et al.*, Lower-current and fast switching of a perpendicular TMR for high speed and high density spin-transfer-torque MRAM, in *2008 IEEE International Electron Devices Meeting* (IEEE, San Francisco, CA, USA, 2008), pp. 1–4.

[88] X. Xie *et al.*, Charge density wave and electron-phonon interaction in epitaxial monolayer $NbSe_2$ films, Chin. Phys. Lett. **38**, 107101 (2021).

[89] B. Guster, C. Rubio-Verdú, R. Robles, J. Zaldívar, P. Dreher, M. Pruneda, J. Á. Silva-Guillén, D.-J. Choi, J. I. Pascual, M. M. Ugeda *et al.*, Coexistence of elastic modulations in the charge density wave state of 2H-$NbSe_2$, Nano Lett. **19**, 3027 (2019).

[90] F. Zheng, Z. Zhou, X. Liu, and J. Feng, First-principles study of charge and magnetic ordering in monolayer $NbSe_2$, Phys. Rev. B **97**, 081101(R) (2018).

[91] X. Xi, Z. Wang, W. Zhao, J.-H. Park, K. T. Law, H. Berger, L. Forró, J. Shan, and K. F. Mak, Ising pairing in superconducting $NbSe_2$ atomic layers, Nat. Phys. **12**, 139 (2016).

[92] C. Sergio, M. R. Sinko, D. P. Gopalan, N. Sivadas, K. L. Seyler, K. Watanabe, T. Taniguchi, A. W. Tsen, X. Xu, D. Xiao *et al.*, Tuning Ising superconductivity with layer and spin–orbit coupling in two-dimensional transition-metal dichalcogenides, Nat. Commun. **9**, 1427 (2018).

[93] H. Matsuoka, M. Nakano, T. Shitaokoshi, T. Ouchi, Y. Wang, Y. Kashiwabara, S. Yoshida, K. Ishizaka, M. Kawasaki, Y. Kohama *et al.*, Angle dependence of H_{c2} with a crossover between the orbital and paramagnetic limits, Phys. Rev. Res. **2**, 012064(R) (2020).

[94] Y. Tanaka, H. Matsuoka, M. Nakano, Y. Wang, S. Sasakura, K. Kobayashi, and Y. Iwasa, Superconducting 3R-$Ta_{1+x}Se_2$ with giant in-plane upper critical fields, Nano Lett. **20**, 1725 (2020).

[95] Y.-T. Hsu, A. Vaezi, M. H. Fischer, and E.-A. Kim, Topological superconductivity in monolayer transition metal dichalcogenides, Nat. Commun. **8**, 14985 (2017).

[96] Y. Wang, L. Deng, Q. Wei, Y. Wan, Z. Liu, X. Lu, Y. Li, L. Bi, L. Zhang, H. Lu *et al.*, Spin-valley locking effect in defect states of monolayer MoS_2, Nano Lett. **20**, 2129 (2020).

[97] J. Lin, T. Han, B. A. Piot, Z. Wu, S. Xu, G. Long, L. An, P. Cheung, P.-P. Zheng, P. Plochocka *et al.*, Determining interaction enhanced valley susceptibility in spin-valley-locked MoS_2, Nano Lett. **19**, 1736 (2019).

[98] L. L. Tao and E. Y. Tsymbal, Two-dimensional spin-valley locking spin valve, Phys. Rev. B **100**, 161110(R) (2019).

[99] W.-B. Zhang, Q. Qu, P. Zhu, and C.-H. Lam, Robust intrinsic ferromagnetism and half semiconductivity in stable two-dimensional single-layer chromium trihalides, J. Mater. Chem. C **3**, 12457 (2015).

[100] H. L. Zhuang, P. R. C. Kent, and R. G. Hennig, Strong anisotropy and magnetostriction in the two-dimensional stoner ferromagnet Fe_3GeTe_2, Phys. Rev. B **93**, 134407 (2016).

[101] H. Matsuoka, T. Habe, Y. Iwasa, M. Koshino, and M. Nakano, Spontaneous spin-valley polarization in $NbSe_2$ at a van der Waals interface, Nat. Commun. **13**, 5129 (2022).

[102] L. Xu, M. Yang, L. Shen, J. Zhou, T. Zhu, and Y. P. Feng, Large valley splitting in monolayer WS_2 by proximity coupling to an insulating antiferromagnetic substrate, Phys. Rev. B **97**, 041405(R) (2018).

[103] L. Wang, Z. Lin, and Y. An, Tunable valley polarization, magnetic anisotropy and dipole moment for layered Janus 2H–VSSe with intrinsic room temperature ferromagnetism, J. Alloys Compd. **854**, 157141 (2021).

[104] M. Abdollahi and M. B. Tagani, Tuning intrinsic ferromagnetic and anisotropic properties of the Janus VSeS monolayer, J. Mater. Chem. C **8**, 13286 (2020).